PCCP

Accepted Manuscript

ROYAL SOCIETY OF CHEMISTRY

www.rsc.org/pccp

Physical Chemistry Chemical Physics
CREATED USING THE RSC LaTeX PCCP ARTICLE TEMPLATE – SEE www.rsc.org/electronicfiles FOR DETAILS
ARTICLE TYPE
www. rsc.org/xxxxxx | XXXXXXXX

Tunability of Hybridized Plasmonic Waveguide Mediated by Surface Plasmon Polaritons‡

Ming-Ming Jiang,†[a] Hong-Yu Chen,†[a,b] Chong-Xin Shan,*[a] and De-Zhen Shen*[a]

Received Xth XXXXXXXXXX 20XX, Accepted Xth XXXXXXXXX 20XX
First published on the web Xth XXXXXXXXXX 200X
DOI: 10.1039/b000000x

Hybrid plasmonic waveguides make a rapid advances in plasmonics that gives rise to remarkable field enhancement, light harvest, light-transport capabilities, thus bridges the gap between electronics and photonics by routing and manipulating light at subwavelength regions and so on. However, the development of plasmonic waveguide is hindered by the lack of devices that can adjust coherent plasmonic fields. In this letter, hybridized planar multilayer insulator metal insulator metal insulator heterostructures have been proposed, and demonstrated that the unique capability can be used to adjust the mode characteristics by means of varying the thickness of insulator spacer layer inserted between two metal films, such as the shift of surface plasmon resonance wavelength. This type of hybrid plasmonic waveguide opens up opportunities for the tunability of mode characteristics, adjustment of resonant energy transfer processes as well, that have the potential to design novel optical micro/nano resonance cavities dramatically.

1 Introduction

Plasmonics provides a route to develop ultracompact optical devices on a chip by using extreme light concentration and the ability to perform electrical and optical functions simultaneously. These properties make plasmonics an ideal candidate for dynamically adjusting photon-electron interactions at nanoscale[1–5]. These relatively novel devices derived from manipulation of surface plasmon polaritons (SPPs)-electromagnetic waves that propagating along a metal surface, such as hybridized plasmonic waveguides, optical nano/mocro cavities based on spasers[6–9]. One of the most remarkable characteristics associated with hybrid plasmonic waveguides, which generated from metal films or quasi-films (localized and propagating plasmons can also be supported by metallic quasi-films) at optical wavelengths, is the tunabilities of electronic collective oscillation[10,11]. Plasmonic waveguides can be applied to break through the diffraction limit, optical field imprisoned by means of dark modes and so on, such as surface enhanced Raman scattering, nanolasing, plasmonic sensing, and enhancement of spontaneous emission[3,4,12,13]. Plasmon lasers have been demonstrated theoretically[14] and experimentally[2,15] with silver (Ag) metal film and semiconductor materials. For instance, based on ZnO nanowire and Ag film, it is difficult to observe the deep subwavelength plasmonic laser action at UV region[2,3,16–21]. The key to the problem may be the mismatch between the lasing of ZnO nanowire ($\sim$ 390 nm) with surface plasmon resonance based on hybrid plasmonic waveguide composed with Ag film.

The local surface plasmon resonance wavelength in metallic nanoparticles is highly dependent on the environment around the nanoparticles, as well as the coupling among the metal nanoparticles and the size of the nanoparticles. An aggregation of metallic nanoparticles also exhibits blue shift in the resonance wavelength changing from red to violet or blue band, so as well as metal films[22–25]. If another metal film was introduced to the hybrid plasmonic waveguide, such as the metal-insulation-metal (MIM) waveguides, which exhibit oscillatory modes for sufficient thickness of the intermediate dielectric core[3,26–29]. The coupling between surface plasmon polaritons at the two core/cladding interfaces changes significantly when the dielectric constants of the sub- and superstrates are different. The MIM waveguides can achieve extreme light concentration and manipulation, which help researchers to distort nanophotonics space and mould the flow of light in an unprecedented fashion, and have very widely used in perfect lens, hyperlens and transformation optics[29–31]. Additionally, MIM plasmonic waveguides can also be used to design novel plasmonic nano/micro-cavities, such as plasmonic Fabry-Perot resonant cavity. Such structures can quantize the energy of photons propagating along the optical axis of the cavity and thereby strongly modify the spontaneous emission prop-

‡ Electronic Supplementary Information (ESI) available: [details of any supplementary information available should be included here]. See DOI: 10.1039/b000000x/

[a] *State key Laboratory of Luminescence and Applications, Changchun Institute of Optics, Fine Mechanics and Physics, Chinese Academy of Sciences, No.3888 Dongnanhu Road, Changchun, 130033, People's Republic of China*
[b] *Graduate University of the Chinese Academy of Sciences, Beijing, 100049, People's Republic of China.*
† These authors contributed equally to this work.
∗ *E-mail: shancx@ciomp.ac.cn, shendz@ciomp.ac.cn*

erties of a photon-emitting medium inside a resonant cavity, metallic fins that reflect most of incident surface plasmon to concentrate light within a subwavelength cavity mode. Therefore, metallic layers can achieve much higher optical field confinement as well as sustaining high Q-factor[9,32,33]. On-chip plasmon-induced transparency based on plasmonic coupled nanocavities can also be obtained due to the U-shaped plasmonic waveguide[28].

Coupled surface plasmon polaritons (CSPPs) induced by double metal films construct plasmonic waveguides are reported to provide effective transfers of field enhancement from the surface of the upper metal film to the spacer (the space between the double layer metal film) on opposite sides of the upper metal films by means of controlling the spacer between two metal films[4,34–36]. The coupled SPPs happened in the spacer can be applied to achieve storage of electromagnetic energy, interspacer for electronic collective oscillation, photonic circuit integration and so on. Therefore, how to adjust the coupling strength, tunability of plasmonic resonance, and dark modes become important carrier for the implementation of plasmonic circuit integration, microminiature plasmonic devices of light emitting diodes (LEDs), laser diodes (LDs) and biological sensing detectors[12,37,38].

In this letter, a new kind of tunable hybrid plasmonic waveguide by introducing another metal film accompanied with a low index dielectric layer between were present. The insulation-metal-insulation-metal-insulation (IMIMI) hybrid plasmonic waveguide structures were studied could be found out the red-shift of plasmonic resonance wavelength from 450 nm to 600 nm, thereby to achieve the tunability of the hybrid plasmonic mode characteristics when placed a high-index dielectric nanowire on the top surface of the IMIMI waveguides with a nanoscale gap. Plasmonic resonant energy transfer processes could be derived from the low-index dielectric spacer, as well as the tunability of mode characteristics. These tunable characteristics can be attributed to the coupling between the cylinder modes and the hybrid plasmonic modes.

2 Tunability of hybridized plasmonic waveguides

On the basis of metal films adopted in the plasmonic waveguide devices, optical SPP waveguides are mainly classified into two categories, IMI-type and MIM-type[39]. Take the IMIMI structure waveguide for example, $\varepsilon_1/\varepsilon_{m1}/\varepsilon_2/\varepsilon_{m2}/\varepsilon_3$, corresponding to the thickness of the layers $d_1, d_{m1}, d_2, d_{m2}, d_3$, here ε_{m1} and ε_{m2} are the dielectric constants of the two different metal films respectively, as shown in Fig. 1. Solving this system of linear equations results in an implicit expression for

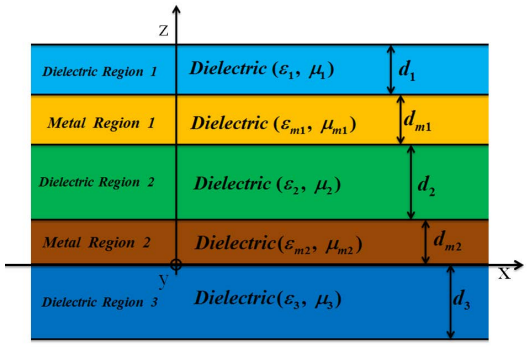

Fig. 1 Geometry of a five-layer system consisting of the IMIMI waveguide with permittivities $\varepsilon_1/\varepsilon_{m1}/\varepsilon_2/\varepsilon_{m2}/\varepsilon_3$, corresponding to the thickness of the layers $d_1, d_{m1}, d_2, d_{m2}, d_3$, here ε_{m1} and ε_{m2} are the dielectric function of the two different metal films respectively.

the dispersion relation linking β and ω via

$$e^{-2k_2d_2} = \frac{\left(1+\frac{\varepsilon_2k_{m2}}{\varepsilon_{m2}k_2}\right)\left(1+\frac{\varepsilon_{m2}k_3}{\varepsilon_3k_{m2}}\right)+\left(1-\frac{\varepsilon_2k_{m2}}{\varepsilon_{m2}k_2}\right)\left(1-\frac{\varepsilon_{m2}k_3}{\varepsilon_3k_{m2}}\right)e^{-2k_{m2}d_3}}{\left(1-\frac{\varepsilon_2k_{m2}}{\varepsilon_{m2}k_2}\right)\left(1+\frac{\varepsilon_{m2}k_3}{\varepsilon_3k_{m2}}\right)+\left(1+\frac{\varepsilon_2k_{m2}}{\varepsilon_{m2}k_2}\right)\left(1-\frac{\varepsilon_{m2}k_3}{\varepsilon_3k_{m2}}\right)e^{-2k_{m2}d_3}} \bullet \frac{\left(1-\frac{\varepsilon_1k_{m1}}{\varepsilon_{m1}k_1}\right)\left(1+\frac{\varepsilon_{m1}k_2}{\varepsilon_2k_{m1}}\right)+\left(1+\frac{\varepsilon_1k_{m1}}{\varepsilon_{m1}k_1}\right)\left(1-\frac{\varepsilon_{m1}k_1}{\varepsilon_1k_{m1}}\right)e^{-2k_{m1}d_{m1}}}{\left(1-\frac{\varepsilon_1k_{m1}}{\varepsilon_{m1}k_1}\right)\left(1-\frac{\varepsilon_{m1}k_2}{\varepsilon_2k_{m1}}\right)+\left(1+\frac{\varepsilon_1k_{m1}}{\varepsilon_{m1}k_1}\right)\left(1+\frac{\varepsilon_{m1}k_1}{\varepsilon_1k_{m1}}\right)e^{-2k_{m1}d_{m1}}},$$

and

$$k_{1(m1,2,m2,3)} = \sqrt{\beta^2 - \varepsilon_{1(m1,2,m2,3)}\frac{\omega^2}{c^2}} \qquad (1)$$

Due to the equation, the effective mode index of the surface plasmon polaritons for double metal films could be obtained, defined as $n_{eff} = \beta/k_0$, by varying the thickness of the second dielectric layer, d_2. When $d_2 \to 0$, the DSPP wave approaches the behavior of DSPP wave for an $\varepsilon_1/\varepsilon_{m1}(\varepsilon_{m2})/\varepsilon_3$ structure; While d_2 is larger than the penetration depth of DSPP wave, the scenario is close to DSPP wave for an $\varepsilon_1/\varepsilon_{m1}/\varepsilon_2$ structure. Based on the analysis, a tunable plasmonic waveguides were construct, along with a high index nanowire placed on the upper metal film with a gap away from the metal layer. When d_2 is large enough, the mode is simplified as previous reports[14,15]. There are three characteristic length scales that are involved when the surface plasmon wave excited at the interface between metal and dielectric films: the propagation length of the SP mode δ_{SP}, the decay length in the dielectric material δ_d, and the decay length in the metal δ_m. In particular, δ_d is typically of the order of half the wavelength of light involved and dictates the maximum height of any individual features, and thus components, that might be used to control SPPs[1]. Therefore, when the gap distance under certain values, the decay length δ_d excited in the dielectric material by two layer of metal films would appear superposition states, which results

in splitting into symmetric and antisymmetric hybrid modes for the hybridized structures. The superposition of the decay wave happened in the spacer can form the coupling between the two metal films [40,41].

2.1 Theoretical analysis of the tunable mode characteristics of the hybridized plasmonic waveguide

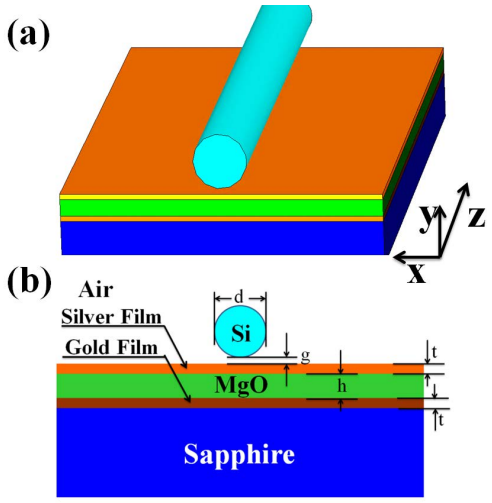

Fig. 2 Geometry of the tunable hybridized plasmonic waveguide: (a) Schematic of the sample; (b) Cross section of hybridized plasmonic waveguide: A dielectric cylindrical nanowire of permittivity ε_c and diameter d is separated from the upper metallic half-space of permittivity ε_{m1} by a nanoscale dielectric gap of permittivity g and width t. The upper medium is a dielectric of permittivity ε_{d1}. The lower metallic half-space of permittivity ε_{m2}, the intermediate low index material permittivity h. $\varepsilon_c = 12.25$ (Si) and $\varepsilon_{d1} = 2.25$ (SiO_2), $\varepsilon_{d2} = 2$, $\varepsilon_{substrate} = 1.56$, at the telecommunications wavelength $\lambda_0 = 1.55\mu m$. The upper metallic region is silver with a permittivity of $\varepsilon_{m1} = -129 + 3.3i$, and the low metallic region is gold with a permittivity of $\varepsilon_{m1} = -110 + 10i$. The centre of the cylinder defines the origin (x=y=0). The surrounding medium is set to be air ($n_{air} = 1$).

In order to understand the tunability of this kind plasmonic waveguide theoretically, a novel hybrid plasmonic waveguides were proposed as shown in Fig. 2 consisting of a high-permittivity semiconductor nanowire (cylinder waveguide) embedded in a low-permittivity dielectric near upper metal surface (double surface plasmon polaritons (DSPP) waveguide) and there is another metal film, separated from the upper metal film with a distance h. An alternative method based on the coupled mode theory [14,15] were employed to describe the mode characteristics of the double metal films. The coupled mode theory applied to describe the mode hybridization of three modes can be referred to the attachment information. Due to the geometry shown in Fig. 2, it could be found that the hybridized model is composed of the cylinder-like mode and double metal films induced DSPP-like modes. Integrated model characteristic parameters would be described as the following three variables, the diameter of high-permittivity semiconductor nanowire d, the gap distance between the high-permittivity semiconductor nanowire and upper metal film g, the gap distance between double metal films h.

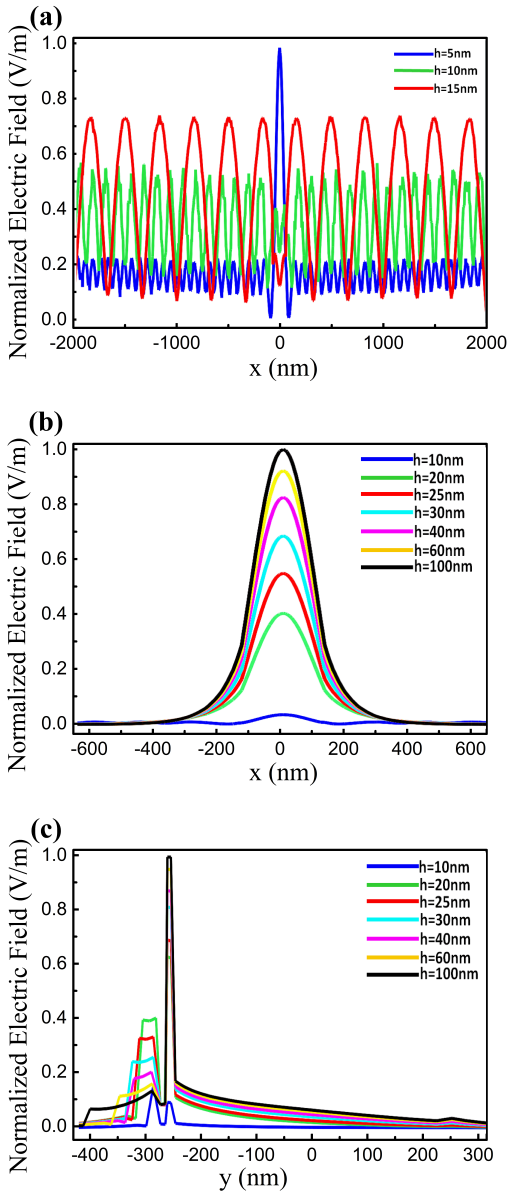

Fig. 3 (a)-(b) Confinement of electric field $E(x,y)$ distribution in the dielectric gap spacer region with $d = 500$ nm, $t = 20$ nm and $g = 5$ nm along y = 0 with the variable spacer thickness h shown in the inset; (c) Confinement of electric field E(x,y) distribution in the dielectric gap spacer region along x = 0 with the variable spacer thickness h.

The thickness effect of metal films has been given in the supply information shown in Figure S5. When the thickness of metal film exceeds 30 nm, metal losses would prevent the surface plasmon energy transfer. Therefore, the tunable mode characteristics of the hybridized plasmonic waveguide would be disappeared. On the contrary, when the thickness of metal films is too thin, the mode characteristics will be uncontrollable. In particular, the silver and gold quasi-films were prepared in the experimental with the thickness about 20 nm. For the sake of the logicality of this letter, the thickness of metal films would be set to be 20nm. Confinement of electric field E(x,y) distribution in the dielectric gap spacer region with d = 500 nm and g = 5 nm along y = 0 and x = 0 were calculated as shown in Figure S2. It demonstrated that when $g = h = 5$ nm, the electromagnetic filed energy was mainly distributed in the dielectric spacer inserted double metal films shown in Fig. S2(a). Electromagnetic field E(x,y) distribution would be transferred from the dielectric spacer to the gap area between the cylinder and the upper metal films when increasing the spacer thickness h, as shown in Fig. S2(b). The critical value of the spacer thickness for the energy storage area transfer is about 25 nm, which is great consistent with the shift of surface plasmon resonance wavelength derived from the change of the dielectric spacer thickness.

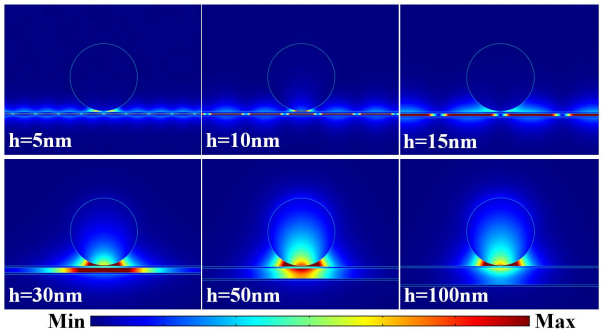

Fig. 4 Electromagnetic energy density distributions with the variable spacer thickness h, where d = 500 nm, g = 5 nm, and t = 20nm.

The spacer thickness h is vital for the electromagnetic field energy distribution, as shown in Fig. 3. When the dielectric spacer thickness is much small, such as in the range of 5 nm $\sim$ 15 nm, the electromagnetic field energy would be mainly concentrated in the dielectric spacer layer derived from Fig. 3(a). In particular, when $h = g$ = 5 nm, evanescent wave excited by the metal films can form the coupling between the cylinder mode and the hybridized plasmonic mode with t = 20 nm. Therefore, a very prominent peak of electromagnetic filed energy distribution can be formed when the dielectric spacer thickness h = 5 nm. When further increasing the spacer thickness (such as more than 15 nm), the confinement of electromagnetic field would be transferred from the dielectric spacer region to the gap area between the cylinder and the upper metal film along y = 0the transfer process detail can be referred to Fig. 3(b). Confinement of electric field $E(x,y)$ distribution in the dielectric gap spacer region along x = 0 demonstrated in Fig. 3(c) can be used as the proof for the shift of the electromagnetic field energy according to the variable spacer thickness h.

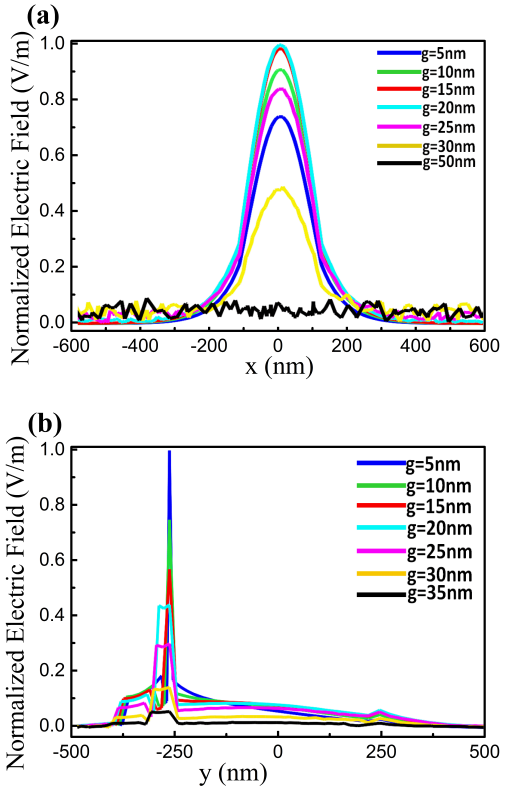

Fig. 5 (a) Confinement of electric field $E(x,y)$ distribution with d = 500 nm and h = 75 nm along y = 0 with the variable gap distance between the cylinder and the upper metal film g shown in the inset; (b) Confinement of electric field $E(x,y)$ distribution along x = 0 with the variable gap distance between the cylinder and the upper metal film g shown in the inset, where the metal film thickness t = 20 nm.

In order to gain a further understanding of the transfer process, at moderate cylinder diameters (d = 500 nm), mode coupling results in the hybridized mode that features both cylinder and SPP characteristics; namely, its electromagnetic energy is distributed over both the cylinder and the adjacent metal-dielectric interface (Fig. 4). However, when increasing the spacer thickness, the hybrid mode would display characteristics of both the cylinder and the SPP mode; Interestingly though, it is strongly confined in two regions: within the gap between the cylinder and the upper metal film, the dielectric

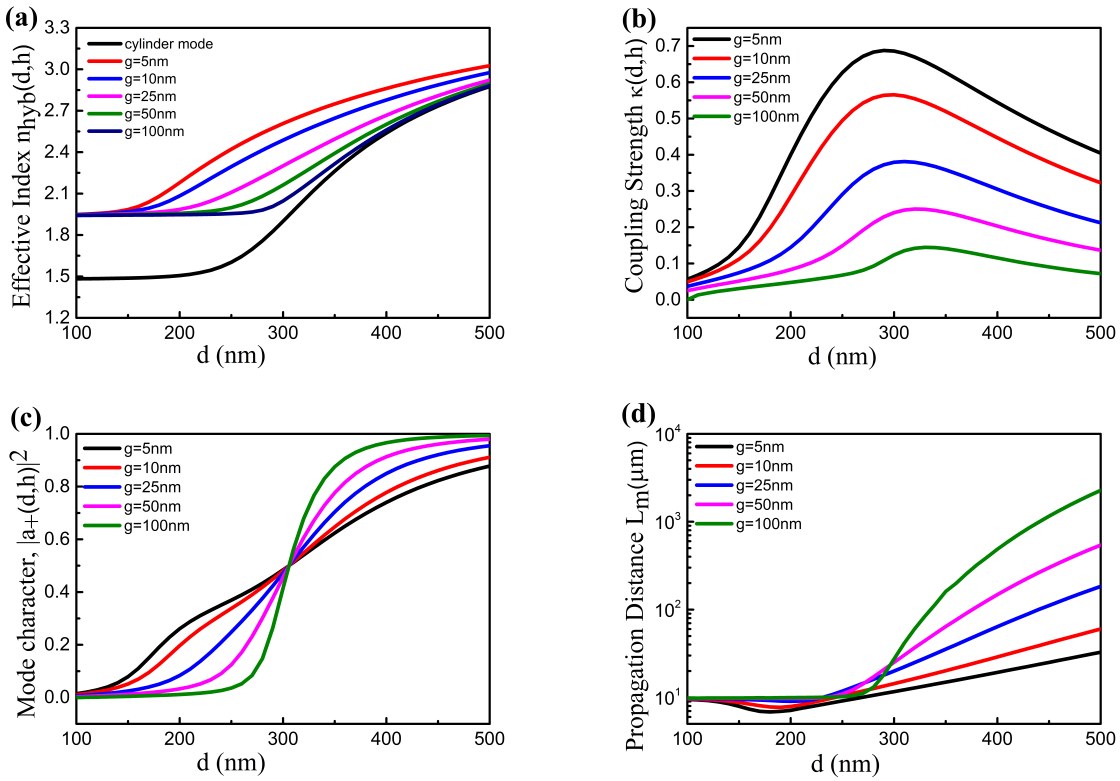

Fig. 6 The mode characteristics of hybridized plasmonic waveguide: (a) The mode effective index of the hybrid waveguide for a range of gap widths g and cylinder diameters d when h = 75 nm, the cylinder mode demonstrated shows significant difference from the hybrid plasmonic modes induced by double metal films; (b) coupling strength $\kappa(d,h)$ dependent on the diameter of the cylinder and the dielectric spacer thickness; (c) When $|a_+(d,h_1)|^2 > 0.5$ the mode is cylinder-like and $|a_+(d,h_1)|^2 < 0.5$, the mode is SPPs-like modes, hence, $|a_+(d,h_1)|^2 = 0.5$ means that the maximum coupling occurs where the hybrid mode consists of equal proportions of cylinder and SPPs modes; (d) The hybrid modes propagation distance L_m.

spacer inserted the two metal films. Therefore, both Fig. 3 and Fig. 4 together, electromagnetic energy density distributions, as well as the transfer process can be expressed clearly with the variable spacer thickness h.

So as to form the hybridized modes consisting of the cylinder-like mode and DLSPP mode, the attention would be focused on the variable of the gap distance g between the cylinder and the upper metal film. Electromagnetic energy density distributions with d = 500 nm and h = 75 nm along y = 0 were calculated as shown in Fig. 5(a). The energy density along y = 0 shows subwavelength localization with variable g from 5 nm to 30 nm. However, when the gap distance exceeds 30 nm, subwavelength localization with variable g will slowly disappear. So as well as the confinement of electric field $E(x,y)$ distribution along x = 0 displayed in Fig. 5(b). Evidently, the gap between the cylinder and the upper metal film, and the dielectric spacer inserted the two metal films between provide the means to store electromagnetic energy, leading to subwavelength optical guiding with low mode loss. This is further confirmed by resolving the electromagnetic energy density in more detail (Fig. 2, Fig. 3 and Fig. 5). Hence, the gap region and the spacer region can be treated as the area of low-permittivity dielectric directly beneath the cylinder and above the metal, and low-permittivity dielectric directly inserted the two metal films. The strong energy confinement in the two regions occurs for two reasons. First, it arises from the continuity of the displacement field at the material interfaces, which leads to a strong normal electric-field component in the gap. Second, in both uncoupled SPP and cylinder geometries, the electric-field components normal to the material interfaces are dominant, amplifying the first effect. In fact, the dielectric discontinuity at the semiconductor-oxide interface produces a polarization charge that interacts with the plasma oscillations of the metal-oxide interface; that is, the gap region has an effective optical capacitance, similar to that of a closely spaced metallic wire and plane.

As a result, for an arbitrary fixed thickness of dielectric spacer layer, the gap distance g separated from the upper metal film of the MIM waveguide should be less than the spacer thickness, the hybrid plasmonic waveguides can provide subwavelength confinement by storing optical energy in the form of electron oscillations within dissipative metallic regions. As slowly increasing the spacer thickness h, the optical energy distribution will transfer from the dielectric spacer region inserted two metal films to the gap between the cylinder and the adjustment metal film area. It is found that the dielectric spacer is capable of realizing the tunability of optical energy distribution by means of adjusting the spacer thickness inserted the two metal films. The strong coupling between the dielectric cylinder mode and the DSPP mode supported at the interface of dielectric environment capped cylinder and the MIM hybridized plasmonic waveguide results in an extremely confined hybrid plasmonic mode, while the evanescent coupling between the upper metal film mode and the low metal film coupling with the substrate acting as a perturbation to the hybrid mode as elaborated below.

Now, in order to further understanding the mode characteristics of the hybrid mode, the attention would be turned to the tunability of mode characteristics, such as the effective mode index, coupling strength, mode character and propagation distance [14,39]. As for fixed the spacer thickness h = 75 nm (h = 50 nm and h = 100 nm can be found in Supplementary Information). According to the coupled mode theory calculated in the Supplementary Information, the effective mode index $n_{hyb}(d,h)$, coupling strength $\kappa(d,h)$ between the cylinder-like mode and DSPP-like mode supported by double metal films induced, the mode character $|a_+(d,h)|^2$ can be used to predict the transition between cylinder-like and SPP-like modes, and the propagation distance $L_m(d,h)$ have been demonstrated in Figs. 6(a)- 6(d). Fig. 6(a) depicts the variation of the effective mode index. Naturally, in the limits of cylinder-like and SPP-like modes, the effective index approaches that of a pure cylinder, $n_{cyl}(d)$, or an SPP, n_{dspp} = 1.9 (h = 75 nm), mode. Compared with the results [14] n_{dspp} = 1.49, the difference is derived from the other metal film. When h = 50 nm, n_{dspp} = 2.14; and h = 100 nm, n_{dspp} = 1.83. Therefore, the spacer thickness h can be used to adjust the n_{dspp}. The coupling strength gets its maximum value when $n_{cyl} = n_{dspp}$ at the critical diameter d_c of the cylinder waveguide, where the cylinder mode and DSPP mode propagate in phase and the effective optical capacitance of the coupled system is maximized, so that the coupling between the two modes is strongest; so as well as the mode character predicted the transition between cylinder-like and SPP-like modes. Variation of the spacer thickness does not only affect the critical diameter d_c of the cylinder waveguide changing from 330 nm to 280 nm, but also the coupling strength changes from 0.6 to 0.75 with h from 50 nm to 100 nm. The propagation distance L_m shown in Fig. 6(d) is also affected by the spacer thickness. The details and tunable mode characteristics of the hybridized plasmonic waveguides can be referred to additional information.

Microminiature nanometer laser based on novel plasmonic devices and hybridized plasmonic waveguides opened a door to overcome challenge of the diffraction limit of light for barrier limits traditional optical components [2,15,42,43]. Metal films treated as a plasmon carrier, an electrical contact, and an effective heat sink has been successfully applied to study plasmonic spaser, the design of plasmonic nanocavity and microcavity [3,23,44]. A further challenge is to achieve directional emission, which is difficult owing to the large momentum mismatch of photons emission and the surface plasmon resonance wavelengths. This kind of tunable hybridized plasmonic waveguide maybe provide new and creative approaches of efficient coupling of coherent nanoscopic light into a waveguide, which could route the light signals to various other devices such as detectors and modulators, as well as modulated plasmonic devices [2,15,16,22,34].

2.2 Tunable surface plasmon resonances of the hybridized plasmonic waveguides

Graphene induced tunability of the surface plasmon resonance have been demonstrated by varying the thickness of Al_2O_3 spacer layer inserted between the graphene and nanoparticles. By varying the spacer layer thickness from 0.3 to 1.8 nm, the resonance wavelength is shifted from 583 to 566 nm [34]. The gap inserted between these two films could provide a platform to achieve the coupling between surface plasmon wave excited by two layer of metal films. However, the integration of plasmonic components based on tunable hybrid plasmonic waveguides has been hampered by the lack of a broader occasion for the coupling between two metal films plasmon guided modes by means of adjusting the spacer distance between two the metal films.

In this letter, gold (99.99%) was first deposited on the c-face sapphire by a radio-frequency magnetron sputtering technique at room temperature with a pressure of 5×10^{-2} Pa, and subsequently annealed in a N_2 atmosphere at 350 $^{\circ}C$ to form gold quasi-film. Then MgO thin film was deposited on the gold quasi-film by MOCVD method, followed silver (99.99%) quasi-film deposited on the MgO film with different thickness of MgO film. By adjusting the MgO film thickness, the red-shifted of plasmonic resonance wavelength from 450 nm to 600 nm was realized shown in Fig. 7. Tunability of the resonance wavelength of local surface plasmon resonance (LSPR) by varying the distance between gold quasi-film and silver quasi-film can be realized. It is estimated that every nanometer of change in the distance between two metal quasi-films corresponds to a resonance wavelength shift of $\sim$ 7.5 nm. The gold and silver quasi-films separation changes the coupling

strength of the electromagnetic field of the excited plasmons in the nanoparticles and the antiparallel image dipoles in silver quasi-film.

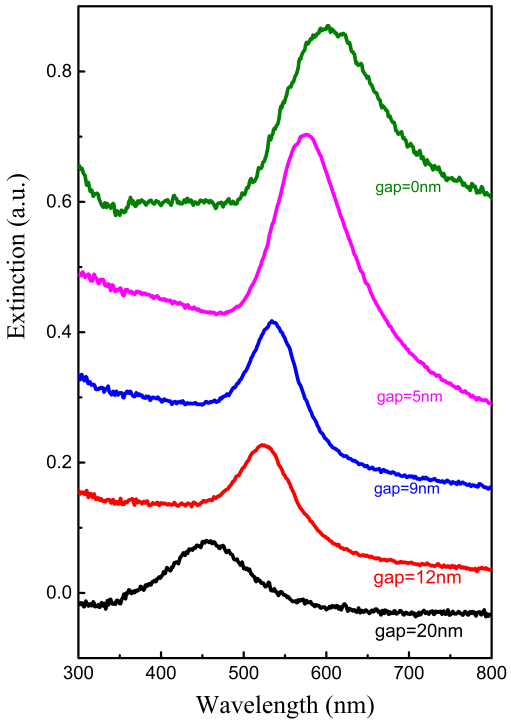

Fig. 7 Extinction spectra of two metal quasi-films mediated tunable surface plasmon resonances with different spacer layer gap, such as 0, 5nm, 9nm, 12nm, 20nm.

Fig. 7 demonstrates that when the double metal film preparation together directly, only the extinction spectra of gold can be observed at about 600 nm. But when increasing the thickness of MgO layer between silver and gold films, the plasmonic resonance wavelength will appear blue-shift. Once the thickness of MgO layer exceeded 20 nm, the plasmonic resonance wavelength of hybridized plasmonic waveguide would stay at around 450 nm. These results are basically identical to our previous studies results of metal nanoparticles and single layer metal film surface plasmon resonance [22,23]. It can be found that by adjusting the thickness of the two kinds of metal films and the thickness of the dielectric layer sandwiched between, tunability of plasmonic resonance wavelength can be achieved. Meanwhile, tunability of plasmonic resonance can also be happened in the short wavelength range with Al metal films [45].

The coupling strength between the evanescent waves excited by the metal quasi-films could be adjusted by means of adjusting the spacer thickness. Since the incident unpolarized light beam is perpendicular to the sample surface, the electric field has no vertical component with respect to the sample surface, which means only lateral electron oscillations in the metal films can be induced. When the spacer distance between double metal films is small, an antiparallel image dipole will be formed in the conducting film. The presence of an antiparallel image dipole will reduce the internal field in the metal films, which results in a red shift of the resonance wavelength and the interaction between the dipoles will decrease as the spacer layer thickness increases. As a result, the resonance wavelength shows a blue shift with increasing the spacer layer. Therefore, our result infers the formation of laterally oscillating image dipoles in Ag film. As proposed theoretically, the laterally oscillating image dipoles introduce less resonance shift as compared to the vertically oscillating image dipoles. To induce the vertically oscillating image dipoles, an electrical field with a component perpendicular to the sample surface must be presented. For this purpose, the sample is tilted for various angles in our experimental setup and the transmission spectra are measured. But no additional resonance dip is observed and there is no observable change in the resonance wavelength compared to the case of zero tilting, suggesting that no vertical oscillating dipole is present in our sample [10,11].

3 Conclusion

The results given in this letter, could provide a novel theoretical foundation for the tunability of the hybridized plasmonic waveguide, which consisting of a tunable low-index dielectric layer as a spacer. When the spacer thickness ranged from $\sim$ 5 to 30 nm, the surface plasmon resonance is red-shifted from 450 nm to 600 nm. Upon adjusting the spacer thickness, effective surface plasmon resonant energy transfer processes assisted plasmon hybridization processes can be realized, as well as the energy transfer between silver plasmon and gold plasmon. When placed a high-index dielectric semiconductor nanowire on the upper metal film, spacer layer inserted two metal films could achieve the tunability of mode characteristics of the hybridized plasmonic waveguides, such as the mode effective index, coupling strength, the mode character, as well as the hybrid modes propagation distance. In the framework of IMIMI hybridized plasmonic systems approach based on plasmonic materials can represent a relevant step forward towards novel applications of integrated plasmon-based circuitry, the potential application of high gain, low threshold plasmonic amplifier and lasers based on different semiconductor nanowires in the future.

Acknowledgements

This work is supported by National Basic Research Program of China (973 Program) under Grant Nos. (2011CB3020022011CB302004), the Key Program of the National Natural Science Foundation of China (11134009), the National Natural Science Foundation of China under Grant Nos. (21101146, 61177040) the 100 Talents Program of the Chinese Academy of Sciences.

References

1 W. L. Barnes, A. Dereux and T. W. Ebbesen, *Nature*, 2003, **424**, 824–830.
2 Y.-J. Lu, J. Kim, H.-Y. Chen, C. Wu, N. Dabidian, C. E. Sanders, C.-Y. Wang, M.-Y. Lu, B.-H. Li, X. Qiu *et al.*, *Science*, 2012, **337**, 450–453.
3 K. Ding and C. Ning, *Light: Sci. Appl.*, 2012, **1**, e20.
4 C. Ciracì, R. Hill, J. Mock, Y. Urzhumov, A. Fernández-Domínguez, S. Maier, J. Pendry, A. Chilkoti and D. Smith, *Science*, 2012, **337**, 1072–1074.
5 D. K. Gramotnev and S. I. Bozhevolnyi, *Nature Photonics*, 2010, **4**, 83–91.
6 W. Cai, A. P. Vasudev and M. L. Brongersma, *Science*, 2011, **333**, 1720–1723.
7 M. Noginov, G. Zhu, A. Belgrave, R. Bakker, V. Shalaev, E. Narimanov, S. Stout, E. Herz, T. Suteewong and U. Wiesner, *Nature*, 2009, **460**, 1110–1112.
8 O. L. Berman, R. Y. Kezerashvili and Y. E. Lozovik, *Phys. Rev. B*, 2013, **88**, 235424.
9 B. Min, E. Ostby, V. Sorger, E. Ulin-Avila, L. Yang, X. Zhang and K. Vahala, *Nature*, 2009, **457**, 455–458.
10 T. Kelf, Y. Sugawara, R. Cole, J. Baumberg, M. Abdelsalam, S. Cintra, S. Mahajan, A. Russell and P. Bartlett, *Phys. Rev. B*, 2006, **74**, 245415.
11 M. Schwind, B. Kasemo and I. Zoric, *Nano Lett.*, 2013, **13**, 1743–1750.
12 Y.-H. Su, Y.-F. Ke, S.-L. Cai and Q.-Y. Yao, *Light: Sci. Appl.*, 2012, **1**, e14.
13 G. Lozano, D. J. Louwers, S. R. Rodríguez, S. Murai, O. T. Jansen, M. A. Verschuuren and J. G. Rivas, *Light: Sci. Appl.*, 2013, **2**, e66.
14 R. F. Oulton, V. J. Sorger, D. Genov, D. Pile and X. Zhang, *Nature Photonics*, 2008, **2**, 496–500.
15 R. F. Oulton, V. J. Sorger, T. Zentgraf, R.-M. Ma, C. Gladden, L. Dai, G. Bartal and X. Zhang, *Nature*, 2009, **461**, 629–632.
16 V. J. Sorger, N. Pholchai, E. Cubukcu, R. F. Oulton, P. Kolchin, C. Borschel, M. Gnauck, C. Ronning and X. Zhang, *Nano Lett.*, 2011, **11**, 4907–4911.
17 M. A. Versteegh, D. Vanmaekelbergh and J. I. Dijkhuis, *Phys. Rev. Lett.*, 2012, **108**, 157402.
18 S. Chu, G. Wang, W. Zhou, Y. Lin, L. Chernyak, J. Zhao, J. Kong, L. Li, J. Ren and J. Liu, *Nature Nanotechnology*, 2011, **6**, 506–510.
19 D. Vanmaekelbergh and L. K. van Vugt, *Nanoscale*, 2011, **3**, 2783–2800.
20 S. Rodriguez, S. Murai, M. Verschuuren and J. G. Rivas, *Phys. Rev. Lett.*, 2012, **109**, 166803.
21 S. Thongrattanasiri and F. J. G. de Abajo, *Phys. Rev. Lett.*, 2013, **110**, 187401.
22 M.-M. Jiang, H.-Y. Chen, B.-H. Li, K.-W. Liu, C.-X. Shan and D.-Z. Shen, *J. Mater. Chem. C*, 2013, **2**, 56–63.
23 M.-M. Jiang, B. Zhao, H.-Y. Chen, D.-X. Zhao, C.-X. Shan and D.-Z. Shen, *Nanoscale*, 2014, **6**, 1354–1361.
24 P. Andrew and W. Barnes, *Science*, 2004, **306**, 1002–1005.
25 Y.-K. Liu, S.-C. Wang, Y.-Y. Li, L.-Y. Song, X.-S. Xie, M.-N. Feng, Z.-M. Xiao, S.-Z. Deng, J.-Y. Zhou, J.-T. Li *et al.*, *Light: Sci. Appl.*, 2013, **2**, e52.
26 S. Feng, X. Zhang and P. J. Klar, *App. Phys. Lett.*, 2011, **99**, 053119.
27 Z. Ye, Y. Peng, T. Zhai, Y. Zhou and D. Liu, *JOSA B*, 2011, **28**, 502–507.
28 Y. Zhu, X. Hu, H. Yang and Q. Gong, *Scientific Reports*, 2014, **4**, 3752.
29 J. A. Schuller, E. S. Barnard, W. Cai, Y. C. Jun, J. S. White and M. L. Brongersma, *Nature Mater.*, 2010, **9**, 193–204.
30 A. Vakil and N. Engheta, *Science*, 2011, **332**, 1291–1294.
31 J. B. Pendry, *Phys. Rev. Lett.*, 2000, **85**, 3966.
32 S.-W. Chang, T.-R. Lin and S. L. Chuang, *Opt. Express*, 2010, **18**, 15039–15053.
33 V. J. Sorger, R. F. Oulton, J. Yao, G. Bartal and X. Zhang, *Nano Lett.*, 2009, **9**, 3489–3493.
34 J. Niu, Y. Jun Shin, Y. Lee, J.-H. Ahn and H. Yang, *App. Phys. Lett.*, 2012, **100**, 061116–061116.
35 A. González-Tudela, P. Huidobro, L. Martín-Moreno, C. Tejedor and F. García-Vidal, *Phys.l Rev. Lett.*, 2013, **110**, 126801.
36 H. Noh, Y. Chong, A. D. Stone and H. Cao, *Phys. Rev. Lett.*, 2012, **108**, 186805.
37 B. Peng, Q. Zhang, X. Liu, Y. Ji, H. V. Demir, C. H. A. Huan, T. C. Sum and Q. Xiong, *ACS Nano*, 2012, **6**, 6250–6259.
38 Y. Gu, S. Xu, H. Li, S. Wang, M. Cong, J. R. Lombardi and W. Xu, *J. Phys. Chem. Lett.*, 2013, **4**, 3153–3157.
39 S. A. Maier, *Plasmonics: Fundamentals and Applications*, Springer, 2007.
40 B. Wang, X. Zhang, F. J. García-Vidal, X. Yuan and J. Teng, *Phys. Rev. Lett.*, 2012, **109**, 073901.
41 F. Schertz, M. Schmelzeisen, M. Kreiter, H.-J. Elmers and G. Schönhense, *Phys. Rev. Lett.*, 2012, **108**, 237602.
42 V. J. Sorger and X. Zhang, *Science*, 2011, **333**, 709–710.
43 X. Shan, U. Patel, S. Wang, R. Iglesias and N. Tao, *Science*, 2010, **327**, 1363–1366.
44 M. T. Hill, M. Marell, E. S. Leong, B. Smalbrugge, Y. Zhu, M. Sun, P. J. van Veldhoven, E. J. Geluk, F. Karouta, Y.-S. Oei *et al.*, *Opt. Express*, 2009, **17**, 11107–11112.
45 M. W. Knight, N. S. King, L. Liu, H. O. Everitt, P. Nordlander and N. J. Halas, *ACS Nano*, 2013, **8**, 834–840.